PUBLICATION V

Parameter optimization of HVOF sprayed nanostructured alumina and alumina-nickel composite coatings

In: Surface & Coatings Technology 2005.
Accepted for publication.

Available online at www.sciencedirect.com
SCIENCE DIRECT
Surface & Coatings Technology xx (2005) xxx – xxx
SURFACE & COATINGS TECHNOLOGY
www.elsevier.com/locate/surfcoat

Parameter optimization of HVOF sprayed nanostructured alumina and alumina–nickel composite coatings

Erja Turunen[a,*], Tommi Varis[a], Tom E. Gustafsson[a], Jari Keskinen[b], Teppo Fält[c], Simo-Pekka Hannula[a,c]

[a]VTT Industrial Systems, Espoo, VTT, P.O. Box 1703, FIN-02044 VTT, Finland
[b]VTT Processes, Tampere, Finland
[c]Helsinki University of Technology, Physical Metallurgy and Materials Science, Espoo, Finland

Received 16 February 2005; accepted in revised form 9 May 2005

Abstract

The use of a dense ceramic layer as an environmental barrier is often limited due to the differences in coefficient of thermal expansion (CTE) between the coating and steel substrate and poor mechanical strength of the ceramic layer. Nanocrystalline composite materials have been recognized to have special mechanical properties, especially improved fracture toughness in bulk form. In this paper, efforts in transferring the same type of improvements into a thermal spray coating have been made. Development of high velocity oxy-fuel (HVOF) spraying of nanocrystalline Al_2O_3- and Al_2O_3–Ni-coatings, where up to ten percent of nickel has been added in order to toughen the coating, is described. Spray parameters were optimized for HV-2000 HVOF spraying system based on the on-line diagnostics and single splat studies. Parameters were selected aiming at different melting stages of the powder. The resulting microstructure of the coatings and effect of it on the coating properties is discussed.

Keywords: Thermal spraying; HVOF; Process optimization; Diagnostic; Alumina; Nanofraction; Mechanical properties

1. Introduction

Thermal spraying is an effective and low cost method to apply thick coatings to change surface properties of the component. Coatings are used in a wide range of applications including automotive systems, boiler components, power generation equipment, chemical process equipment, aircraft engines, pulp and paper processing equipment, bridges, rollers and EAF electrodes in steel mills, concrete reinforcements, orthopedics and dental, land-based and marine turbines, ships, etc.

Ceramic coatings offer an interesting alternative to produce a protective layer over a steel structure due to their excellent chemical, corrosion and thermal resistance. Plasma spraying is the most widely used method to produce a thick ceramic coating. Recently it has been shown that HVOF process can produce much denser coatings and hence better environmental protection capacity than plasma sprayed coatings [1–3].

Poor mechanical strength as well as mismatches in coefficient of thermal expansion (CTE) often limits the use of dense ceramic coatings on metals. However, increasing porosity would decrease the protection capability of the coating. It is already recognized that nanocrystalline materials have special mechanical properties. Typically the strength of crystalline materials is increased with decreasing grain size and materials with small grain size often exhibit also superplastic behavior at elevated temperature. Nanocrystallinity has a positive influence on toughness of ceramic materials especially if alloyed with nanophased metals [4–6]. Furthermore, hardness and wear properties of coatings are usually improved. There are several recent reviews on mechanical properties of nanocrystalline materials [7–9].

* Corresponding author. Tel.: +358 20 722 5425; fax: +358 9 463 118.
E-mail address: erja.turunen@vtt.fi (E. Turunen).

0257-8972/$ - see front matter © 2005 Elsevier B.V. All rights reserved.
doi:10.1016/j.surfcoat.2005.05.018

The main effort that has been made so far in the field of nanostructured thermal spray materials has focused on the development of HVOF sprayed metallic or cermet coatings and atmospheric plasma spraying (APS) sprayed ceramic coatings [10,11]. The ceramic coating research is mainly focused on development of APS alumina–titania coatings, which possess superior toughness and adhesion along with high wear and spallation resistance [12–15].

Due to the higher kinetic energy, shorter dwell time of particles in the flame and lower flame temperature compared to the plasma spray, HVOF offers an interesting combination to produce dense coatings with less phase transformations [16]. However, thermal spraying is a very complex process including a number of variables. Particle melting stage and possible phase transformations during particle flight in the thermal spray flame must be controlled, as well as coating build up mechanism including splat interface and stress stages. Different tools have been developed in order to better understand the deposit formation and its relationship to the coating properties. These tools are currently presented under a concept of "Process Map" [17]. It can be considered to have two different meanings aiming either a) the optimization and mapping of different in-flight process conditions of particles producing different melting stages for particles or b) explaining the effect of different splat structures and substrate conditions on the final structure and properties of the deposited coating. These two maps have lately been named as "First order map" and "Second order map" [17].

In order to produce a coating with desired properties, e.g. with high fracture strength, it is not sufficient to control only material structure inside one lamella. Interaction between lamellae, stress stages of the final coating, adhesion to the substrate and cracking must be also controlled. These different phenomena which influence the final quality of the coating are depicted schematically in Fig. 1.

In this work the HVOF coating process for producing nanocrystalline Al_2O_3- and Al_2O_3–Ni-coatings is described. Focus is on the process control, lamellae microstructure, lamellae interaction and their effect on mechanical coating properties, such as hardness, wear resistance and fracture toughness.

2. Experimental procedure

2.1. Spray powder development

Various ways to produce ceramic nanocomposite powders exist. In the present work the synthesis of Al_2O_3 powder with and without Ni-nanoparticles was carried out using boehmite (AlO(OH)) as a starting media. The process is initiated by diluting $Ni(NO_3)_2$ to ethanol and then adding AlO(OH). The amounts are chosen to give the required Ni/Al_2O_3 ratio. After drying the resulting powder is calcined at 500 °C for 2 h to obtain NiO–γ-Al_2O_3. Both nickel oxide and alumina are as nanosized particles.

After calcinations nanopowder particles were agglomerated into larger agglomerates by spray drying. After agglomeration the powder was heat treated in argon containing hydrogen to reduce NiO to metallic nickel and to transform γ-alumina to α- or θ-alumina and to sinter particles together. The temperature used was 1100 °C for 3 h. The temperature was limited to this due to the limitations in the furnace equipment. For some powder batches heat treatment and reduction were performed simultaneously in

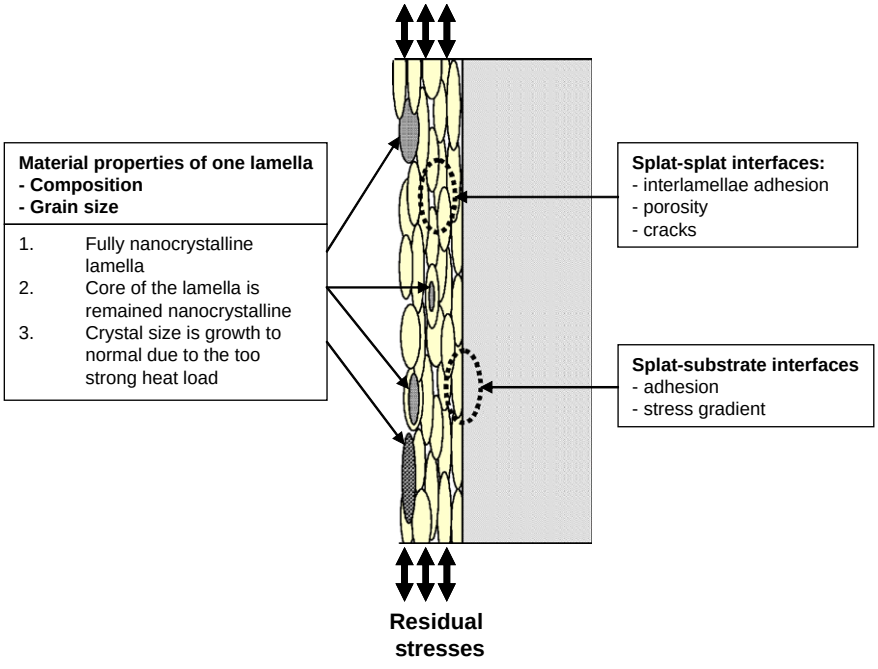

Fig. 1. Factors effecting on the properties of thermally sprayed coating.

hydrogen containing atmosphere. Two powders were produced having nickel content of 2 vol.%, and 5 vol.%, respectively.

Pure nanostructured alumina powders were also manufactured from boehmite. Boehmite was agglomerated by spray drying, heat treated to alumina and finally sintered. This process was similar to the one used for Ni containing alumina. Praxair Al-1110HP Al_2O_3 powder was used as reference material having grain size in the micrometer range.

2.2. Thermal spray test setup

Coatings were deposited using Praxair HV-2000 spray gun fitted with 22-mm combustion chambers. Nitrogen was selected for a carrier gas along with hydrogen as a fuel gas. As known from previous studies use of hydrogen results in a narrower process window in terms of velocity and temperature range as compared to propane or propylene [3]. This causes less variation in particle melting stage between different spray conditions. In the current work it was essential to maximize splat interface and therefore, despite the fact of smaller process window, hydrogen was selected as a fuel gas.

A two-axis traverse unit was used to manipulate the gun during coating deposition. Use of Thermico CPF-2HP powder feeder ensured sufficient powder feed rate also for trial powders, which had a non-optimal size distribution having particles smaller than 5 μm in diameter and consequently poor flow capability.

2.3. Online diagnostic studies

Online diagnostics using Spraywatch 3i equipment were carried out at different spray conditions to measure the particle velocity and temperature. Distance of the camera from the spray gun was equal with standoff distance during coating manufacturing being 150 and 200 mm. The measurement is based on the two-colour pyrometry and a fast CCD camera [18]. In diagnostic tests, the total gas flow rate was kept constant and the amount of hydrogen and oxygen was varied to obtain different gas ratios from 2.0 to 2.85. Besides the gas ratio, total gas flow and standoff distance were varied. Two total gas flow rates, 1050 l/min and 890 l/min, were used. Standoff distances of the spray gun from the substrate plate were either 150 or 200 mm.

2.4. Single splat studies

Single splats were collected onto preheated (200 °C) stainless steel substrates in order to study the melting level of the particles in different spray conditions. Splats were produced by spraying with a low powder feed rate over polished steel plates through a special shutter system. By using a shutter system, flame contacted with the steel plate only for some milliseconds, and single splats could be collected within the flame diameter. While temperature data from diagnostic tests, based on emissivity of particle in-flight, provides only the surface temperature of the particle, single splats enhance our understanding on the overall melting stage of a particle. In a case of a material with high melting point and short dwell time in the flame, the surface temperature will not always give the information of the melting through the whole particle.

2.5. Coating deposition

Coatings were sprayed onto grit blasted carbon steel plates having a size of $25 \times 50 \times 2$ mm. Traverse speed of the gun was 0.2 m/s, and approximately 13 μm thickness per pass was deposited. These samples were used for microstructural and property characterization. The spray parameter combinations were similar for the splat and coating deposition and were selected based on the measured on-line diagnostic data.

2.6. Characterization

The crystal structures of the powders and the coatings were characterized by X-ray diffraction (XRD) using Cu-Kα and Mo-Kα radiation. Powder agglomerate size was determined by using Lecotrac — LT100 particle size analyzer. Electron microscopy using JEOL JSM-6400 (SEM) combined with PGT PRISM 2000 X-ray analyzer, LEO982 Gemini (FEG–SEM), and Philips CM 200 (FEG–STEM) combined with Noran Voyager X-ray analyzer were used to study the splats and coating microstructures and to characterize micro-cracking and nickel distribution on fracture surface.

Splats produced with selected spray conditions were studied in detail for their size and thickness. Image analysis and direct length measurements (ImagePro®, Graftek) from images 1260×922 pixels) were applied to measure the diameter of the splats. The SEM was calibrated in X and Y directions with a reference grid (12.5 μm reference distance). The error in length measurements was less than ±3%. The thickness of the splats was derived from X-ray spectra acquired with three acceleration voltages (18, 25, and 33 kV) with constant microscope parameters and X-ray detection geometry. Splat thickness was calculated from Fe-K_α and Al-K_α intensity K-ratios (I_x/I_{std}) as a function of acceleration voltages using a simulation program (X-film®, Synergie[4]) to find the best fit between theoretical curves and experimental data points.

Hardness of the coatings was determined by Vickers micro hardness method using a mass of 300 grams. Instrumented nanoindentation with a Nanotest 550 instrument equipped with a 0.79 mm ball indenter was used to characterize the elasto-plastic properties of the coating. Calculation of elastic modulus was made by using the method developed by Field and Swain [19,20]. Wear resistance of the coatings was evaluated by rubber wheel abrasion test according to standard ASTM G 65-91.

3. Experimental results

3.1. Powder microstructure

After agglomeration and sintering powders were analyzed to confirm the grain size and phase structure of the particles before HVOF spray tests. Powders were analyzed by XRD to consist θ- and α-alumina and nanosized Ni-particles. Powder fraction was measured to be between 2 and 26 μm. Detailed information of the produced powders and a reference powder are presented in Table 1. Typical morphology and cross-section for the particle is presented in Fig. 2.

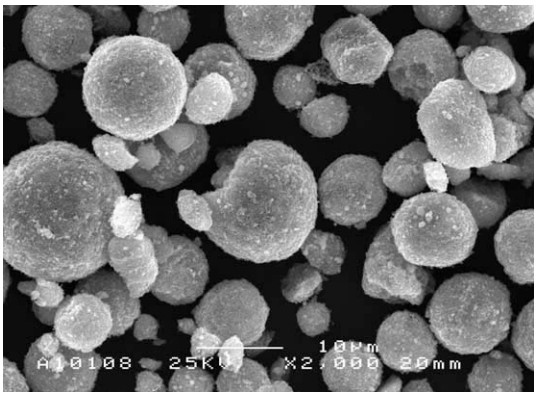

Fig. 2. Typical morphology for the n-Al_2O_3 agglomerates.

3.2. On-line diagnostics

Over 20 different spray conditions were studied where gas ratio of hydrogen and oxygen was varied. Table 2 gives the main trends observed in the measurements.

3.3. Splat studies

Single splats were sprayed on stainless steel at all process conditions using the reference powder. It was found that maximum velocity obtained in condition C is not optimal due to the larger fragmentation of the splat. This will produce small, solidified droplets in the coating, which will disturb the interlamellar adhesion. More detailed analyse were carried out for spray conditions A, B and D. The SEM images of the collected splat populations, and splat outlining by image analysis for size measurements, as well as the structure of corresponding coating cross-section for each spray condition are presented in Fig. 3. Sixteen (16) splats per plate were analyzed in detail for their diameter and thickness.

The average thickness was found to be 0.55 μm for condition A, 0.76 μm for condition B, and 0.48 μm for condition D. Results confirm the visual observations and diagnostic data, showing lowest flattening at condition B due to the lowest particle temperature and velocity. Flattening of the particles increased (thickness decreased) with increasing particle velocity and temperature being highest for condition D. The medians of the splat diameters were 19.25 μm for condition A, 18.8 μm for condition B, and 19.8 μm for condition D. The trend was opposite to that of diameters as expected. Diameter was smallest with the condition B where splat thickness was highest. In all cases, the largest particles have not attached to the substrate. Partly, this is assumed to be caused by the polished surface, and partly by the semi-molten state of the larger particles.

3.4. Coating microstructure

Coatings were deposited from all powders listed in Table 1, using spray conditions A, B and D. Based on the splat tests, spray conditions A and D were expected to be the potential ones to produce good, well adhering coatings. Condition B was selected in order to study the effect of the lower particle velocity and less flattening of the particles on the coating microstructure and properties.

Coating microstructure was studied and analyzed from the polished cross sections of the coatings by SEM in BEI mode, which ensures good contrast for studying flattening rate of the particles and adhesion of the lamellas.

Microstructural analysis based on the microscopy of the coating cross sections showed that coatings A and D, produced a much denser coating structure than spray condition B. The same trend was observed for all spray materials. Densest structures were obtained by using spray condition D. Microstructures for the reference materials with each condition are presented in Fig. 3.

Relative contents of α and γ phases as measured by XRD for ref-Al_2O_3 were 15% and 85% for coating A, 14% and 86% for coating B, and 4% and 96% for coating D. Again a good correlation between diagnostic studies and splat studies was found. A large difference in the alpha content was found between coatings A and D. Despite the higher particle surface temperature in condition A the particle velocity is also higher. Due to this, the dwell times of the particles are shorter in the flame and less melting occurs. This is manifested by the on average less flat single splats as

Table 1
Spray powders for the HVOF experiments

Powder	Material code	Manufacturer and method	Agglomerate size [μm]	Crystal size	Phase structure
Al-1110	ref-Al_2O_3	Praxair, fused and crushed	5–22	Conventional	alpha
Boehmite	n-Al_2O_3	VTT, agglomerated and sintered	2–25	Nano range	alpha
Boehmite	n-Al_2O_3–2% Ni	VTT, agglomerated and sintered	4–23	Nano range	theta
Boehmite	n-Al_2O_3 –5% Ni	VTT, agglomerated and sintered	2–26	Nano range	theta

Table 2
Diagnostic data for different spray conditions

Spray condition	Ratio H_2/O_2	Total flow [l/min]	Standoff [mm]	T [°C]	v [m/s]
A	2.85	1050	150	2050±5	1025±25
B	2.85	1050	200	1989±6	874±69
C	2.48	1050	150	2040±3	1073±34
D	2.00	1050	150	1990±4	1014±7
E	2.85	890	150	2027±5	1003±14

well as by the higher alpha alumina content in the final coating.

For n-Al_2O_3, α/γ ratio was 9%/91% for coating A, 8%/82% for coating B, and 3%/97% for coating D. These results correspond well to the results obtained from the single splat studies. Due to the agglomerated structure of n-Al_2O_3 particles compared to the fused and crushed reference powder, the melting is higher even with spray condition B.

A coating microstructure inside one lamella was studied by high-resolution SEM. A high resolution SEM image of the fracture surface of n-Al_2O_3 coating (D) is shown in Fig. 4. Alumina grains having dimensions in a range of hundreds nanometers are observed. It should be noted that the fine structure seems to have been retained in spite of extensive melting of the powder in the HVOF process and only a small amount of α-Al_2O_3 in the structure.

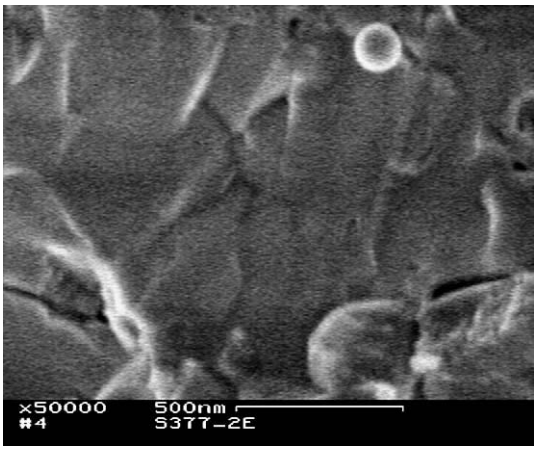

Fig. 4. An FEG–SEM micrograph of a fracture surface of n-Al_2O_3–HVOF coating.

The distribution of nickel in the polished cross sections of the samples as revealed by the back-scattered electron imaging is shown in Fig. 5(a) to (f). These micrographs indicate that nickel is partly deposited into the splat boundaries, i.e. interlamellarily. Especially in the case of 5% of nickel alloy, clear interlamellar deposits of nickel can been observed. A fraction of nickel seems to remain within the lamellae in the nano scale, while some of the nickel is transferred to the interlamellar boundaries, and some is lost in the HVOF spray process. The total nickel content as

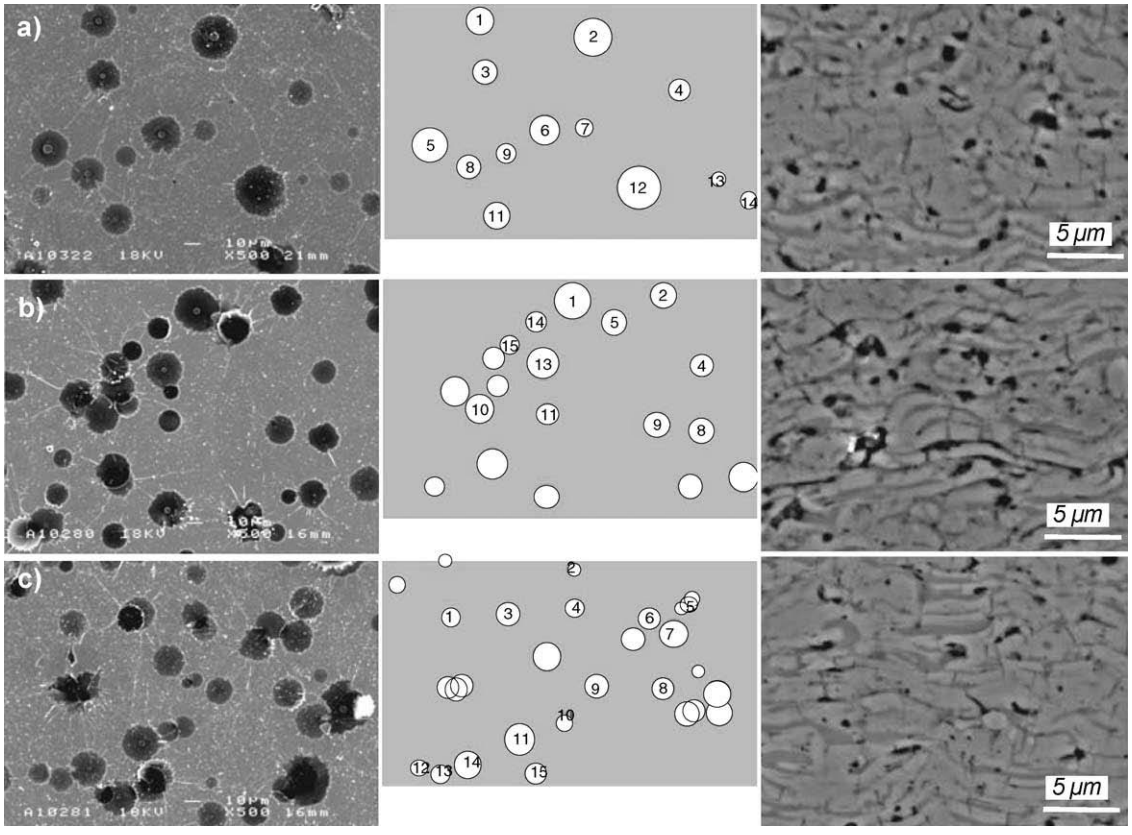

Fig. 3. The SEM images of the collected splat populations, and splat outlining by image analysis for size measurements, as well as the structure of corresponding coating cross-section for each spray condition: a) condition A, b) condition B, c) condition D.

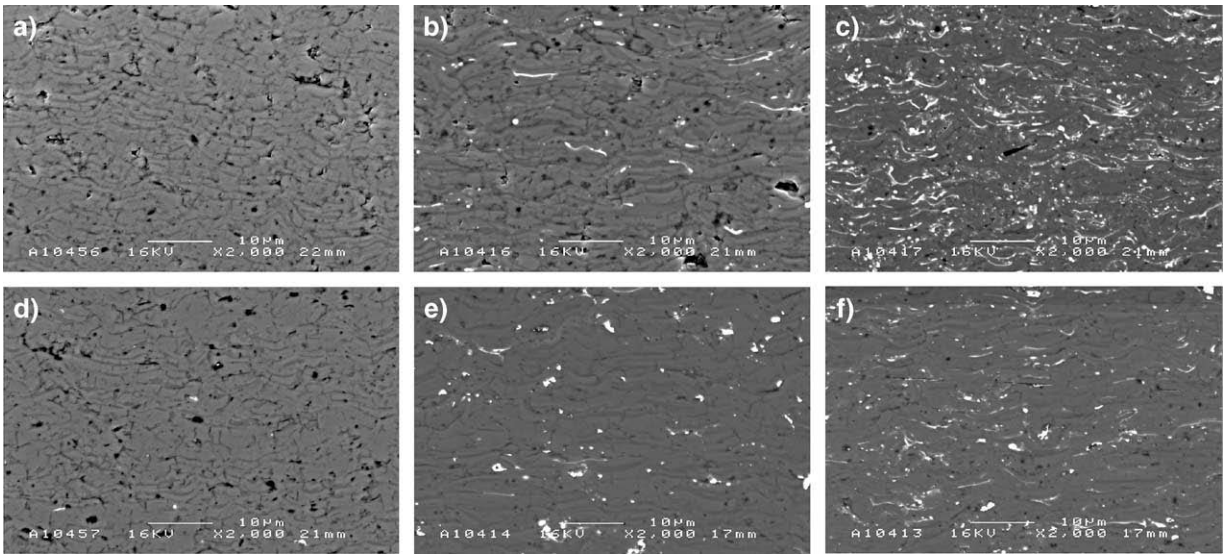

Fig. 5. SEM–BEI micrograph of the polished cross-sections for the coatings sprayed with different spray parameters: a) n-Al_2O_3 (A), b) n-Al_2O_3–2%Ni (A), c) n-Al_2O_3–5%Ni (A), d) n-Al_2O_3 (D), e) n-Al_2O_3–2%Ni (D), f) n-Al_2O_3–5%Ni (D).

measured by EDS from the cross section of the coating showed that the content of the nickel varied depending on the spray parameters. Loss of nickel was the highest in spray condition D, being 34% for the starting powder containing 5% nickel. For condition A the loss was 10%, and for condition B it was 19%. A detailed spot analysis from the alumina matrix, where nickel was not observed visually from the BEI image showed that spray conditions also influenced the content of nickel within the lamellae. The content of the intralamellar nickel was 2.8% for coating I, 3.1% for coating II and 2.3% for coating III, respectively.

Decrease of nickel content was also observed in X-ray diffraction of the coating produced in condition D. The XRD diffraction curve for the coatings sprayed from the powder alloyed with 2% of nickel is presented in Fig. 6. The loss of nickel when using spray condition D can clearly be observed.

3.5. Coating properties

Mechanical properties of the coatings were determined by abrasive wear resistance tests, hardness measurements, and by measuring cracks formed around a Vickers indentation after hardness measurements. A summary of the mechanical properties of the coatings is given in Fig. 7(a) to (c). In Fig. 7(a) Vickers hardness numbers of the coatings are presented. Hardness is highest for the n-coatings sprayed with condition D that was the condition

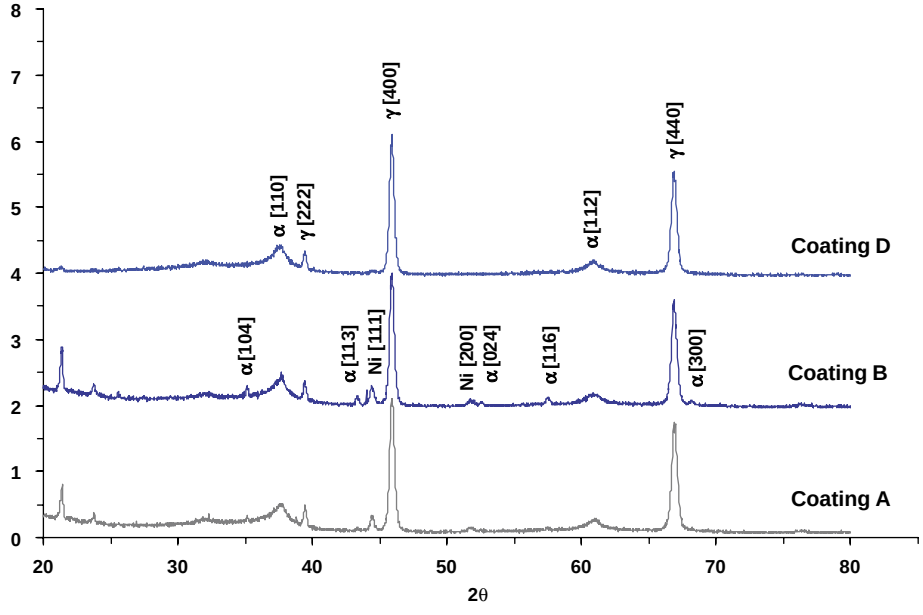

Fig. 6. X-ray diffraction curve for the coatings manufactured from the n-Al_2O_3–2%Ni powder with different spray conditions.

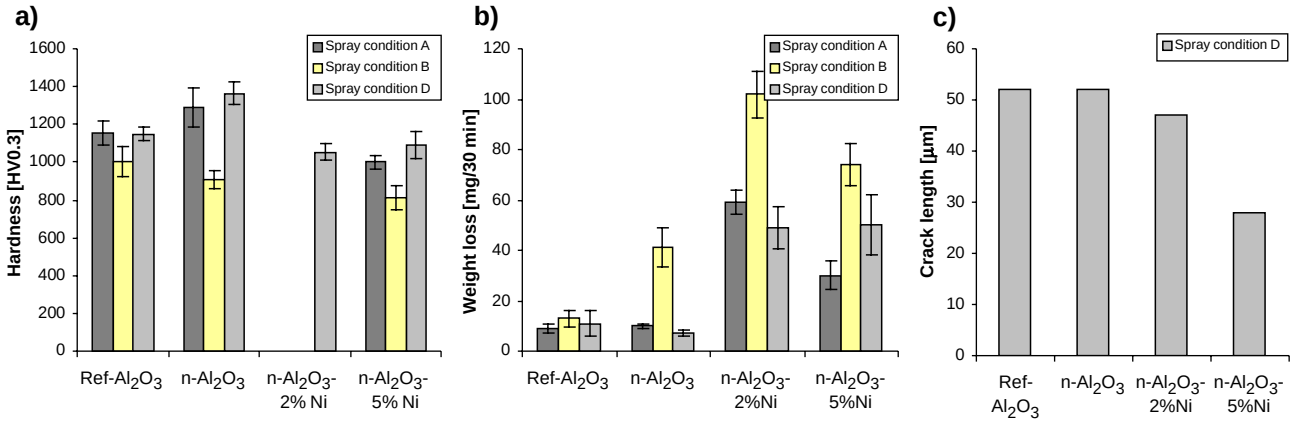

Fig. 7. a) Vickers hardness (HV0.3), b) weight loss in rubber wheel abrasion test, and c) cumulative length of horizontal cracks around a Vickers indentation.

producing thinnest flats. For reference material hardness is equal for spray conditions A and D. Comparison between pure nanoalumina coating (n-Al_2O_3) and the reference coating shows that the hardness is higher for n-Al_2O_3 coatings. This is believed to arise from the use of nanocrystalline feedstock, which results in the refinement of the coating microstructure. However, introduction of nickel into the coating again decreases the hardness.

In order to qualitatively estimate the toughness of the coatings the cumulative length of horizontal cracks around a Vickers indentation (HV0.3) at coating cross sections was measured. The length of cracks is found to decrease with increasing Ni-content as shown in Fig. 7(c).

4. Discussion

In on-line spray diagnostic measurements maximum particle temperatures were detected when the hydrogen/oxygen ratio was either 2.48 or 2.85. This correlates well with the previously reported measurements [3] carried out with same spray set up. Increase of spray distance from 150 mm to 200 mm by keeping other spray conditions constant decreases the surface temperature of the particle. The increase of total gas flow rate has the same effect. Also a decrease in H_2/O_2-gas ratio towards the theoretical stoichiometric value of 2.0 decreases the surface temperature of the particle.

The measured particle velocities around 1000 m/s are quite high as compared to those reported before [3] where maximum velocities were around 800 m/s. This discrepancy results from the used diagnostic equipment. Presently used equipment, Spraywatch, is capable to measure only those particles that are bright enough. In the case of ceramics this means that mainly small particles having higher velocities are measured. The diagnostic system, DVP-2000, which is used in Ref. [3] is capable to measure all particles thus giving lower medium particle velocities. However, the results give the trend between different spray conditions. Highest velocities were measured for the hydrogen/oxygen ratio of 2.48 and 2.85. The velocity decreased when spraying distance was increased or H_2/O_2-gas ratio was decreased. Also, lower total gas flow rate decreased particle velocity.

Splat studies show that flattening rate correlates well with the diagnostic studies. E.g., low particle temperature and velocity is observed for the condition B because of longer spray distance. On the other hand, despite the higher particle temperature in the condition E, the melting stage is lower than in condition B due to the higher particle velocity and shorter dwell time of the particle in the flame. XRD analyses support the results obtained from the diagnostic and splat studies. The amount of alpha phase is smaller when condition D is used. Splat studies and XRD studies show also that melting of the agglomerated nanofraction powder is higher compared to the reference powder, which is fused and crushed. Already, spray condition A produces a denser coating with a lower amount of alpha phase when the nanostructured powder is used instead of the reference powder. According to the splat studies this is a result of improved melting of the agglomerated nanostructured powder at spray flame as compared to that of the fused and crushed reference powder.

The alpha alumina content of the resulting coating is relatively low in all spray conditions. As known from a previous study on alumina coatings [21], alpha alumina content is always low in thermally sprayed coatings due to the fast cooling of the particles. This may have an influence on the mechanical properties of the coating. However, when aiming at good environmental protection properties it is more important to ensure good lamellar bonding and dense structure for the coating. Also, while attempting to increase coating fracture toughness by modifying coating microstructure inside one lamella, the bonding between lamellae must be good enough in order to obtain the improved properties over the complete coating structure. Otherwise, the lamella interface will dominate the overall behavior for the coating despite the microstructure. Therefore, in selection of spray parameters those resulting in good interlamellar bonding should be prioritized over those resulting in high alpha/gamma ratio.

Coatings sprayed in conditions A and D had dense structures. Correlation between flattening rate and coating microstructure for the coating hardness values is obvious. Wear resistance of the coatings (Fig. 7(b)) seems to have a similar dependency on the type of the coating as the coating hardness. While the wear resistance of ceramic coatings is sometimes related to its fracture toughness [22] it seems that in these current materials wear resistance depends rather on the coating hardness and therefore decreases with increasing nickel content.

By using spray condition D, a dense coating structure is obtained with high hardness and good wear resistance. This is believed to correlate with good interlamellar adhesion. Especially in the case of n-Al_2O_3 powder, coating III produced using spray parameter D seems to be superior. Despite the fact that conditions A are "hottest", the dwell time in the flame is shorter and no complete melting has occurred. This can be observed from the α/γ ratio as well as from the coating microstructure. Due to the lower particle velocity in condition B, the coating II has a porous structure and obviously lower interlamellar adhesion resulting in poor wear behaviour. More similarity in coating properties despite the used spray conditions was observed for reference powder. The spray process for the reference material seems to be more robust, which might be caused by denser structure of the fused and crushed powder.

The introduction of nickel into the coating resulted in more variations in the coating structure at different spray conditions. The condition D seems to result in a more radical redistribution of nickel of the original powder into the coating because of the higher melting stage of the particles in this spray condition. Amount of nickel is lower in these coatings both inside the alumina matrix as well as at the lamella boundaries. This has an effect on the mechanical properties of the coating. Especially in the case of n-Al_2O_3–5%Ni the weight loss in abrasive wear test of the coating is increased if the coating is sprayed by using parameter D.

In summary, by introducing nickel into the coating, the fracture toughness seems to improve but simultaneously the hardness and abrasive wear resistance are decreased.

5. Conclusions

In this paper the development of Al_2O_3 and Al_2O_3–Ni HVOF sprayed nanocomposite spray powders and coatings has been described. It was found that by optimizing spray parameters high quality coatings can be obtained.

Introduction of nanopowders to the coating process improves the hardness and wear resistance of the pure Al_2O_3-coating. Introduction of nickel alloying decreases hardness and wear resistance of the coatings, but increases toughness of the coatings.

By adding a small amount of nickel into alumina a coating with high hardness and good fracture toughness is produced. This type of coating is considered to be a potential candidate for a protective coating in the harsh environments where good fracture toughness combined with excellent chemical and corrosion resistance of ceramics is needed.

Acknowledgement

This work was sponsored by TEKES, The National Technology Agency of Finland, VTT Industrial Systems and Finnish industries (Kemira Pigments Oy, Fortum Oil Oy, Rautaruukki Oyj, OMG Kokkola Chemicals Oy, Outokumpu Research Oy, ABR Innova Oy, Pikoteknik Oy, Ionhawk Oy, and Stratum Oy).

References

[1] A.J. Sturgeon, et al., British Ceramic Proceedings, vol. 54, 1997, p. 57.
[2] A. Kulkarni, J. Gutleber, S. Sampath, A. Goland, W.B. Lindquist, H. Herman, A.J. Allen, B. Dowd, Mater. Sci. Eng., A Struct. Mater.: Prop. Microstruct. Process. 369 (2004) 124.
[3] E. Turunen, T. Varis, S.-P. Hannula, A. Kulkarni, J. Gutleber, A. Vaidya, S. Sampath, H. Herman, Mater. Sci. Eng. (submitted for publication).
[4] Y.K. Jeong, K. Niihara, Nanostruct. Mater. 9 (1997) 193.
[5] Masahiro Nawa, Noriko Bamba, Tohru Sekino, Koichi Niihara, J. Eur. Ceram. Soc. 18 (3) (1998) 209.
[6] Sung-Tag Oh, Mutsuo Sando, Koichi Niihara, Scr. Mater. 39 (1998) 1413.
[7] S.-P. Hannula, J. Koskinen, E. Haimi, R. Nowak, in: H.S. Nalwa (Ed.), Encyclopedia of Nanoscience and Nanotechnology, vol. 5, American Scientific Publishers, USA, 2004, p. 131.
[8] M.J. Mayo, Nanostruct. Mater. 9 (1997) 717.
[9] A. Mohammed, Y. Li, Mater. Sci. Eng. 298A (2001) 1.
[10] R. Goswami, H. Herman, S. Sampath, X. Jiang, Y. Tian, G. Halada, Surf. Coat. Technol. 141 (2001) 220.
[11] S.D. Parukuttyamma, J. Margolis, H. Liu, J.B. Parise, C.P. Grey, S. Sampath, P. Gouma, H. Herman, Materials Research Society, Solid-State Chemistry of Inorganic Materials, vol. III, 2001, p. GG6.29.1, USA.
[12] M. Gell, E.H. Jordan, Y.H. Sohn, D. Goberman, L. Shaw, D. Xiao, Surf. Coat. Technol. 146–147 (2001) 48.
[13] E.H. Jordan, M. Gell, Y.H. Sohn, D. Goberman, L. Shaw, S. Jiang, M. Wang, T.D. Xiao, Y. Wang, P. Strutt, Mater. Sci. Eng. 301 (2001) 80.
[14] D. Goberman, Y.H. Sohn, L. Shaw, E. Jordan, M. Gell, Acta Mater. 50 (2002) 1141.
[15] L.L. Shaw, D. Goberman, R. Ren, M. Gell, S. Jiang, Y. Wang, T.D. Xiao, P.R. Strutt, Surf. Coat. Technol. 130 (2000) 1.
[16] R.S. Lima, B.R. Marple, Surf. Coat. Technol. (in press) (available online February 1, 2005).
[17] S. Sampath, X. Jiang, A. Kulkarni, J. Matejicek, D.L. Gilmore, R.A. Neiser, Mater. Sci. Eng., A Struct. Mater.: Prop. Microstruct. Process. 348 (2003) 54.
[18] J. Vattulainen, E. Hämäläinen, R. Hernberg, P. Vuoristo, T. Mäntylä, J. Therm. Spray Technol. 10 (1) (2001) 94.
[19] J.S. Field, M.V. Swain, J. Mater. Res. 8 (1993) 297.
[20] J.S. Field, M.V. Swain, J. Mater. Res. 10 (1995) 101.
[21] D.A.J. Ramm, T.W. Clyne, A.J. Sturgeon, S. Dunkerton, Correlations between Spray Conditions and Microstructure for Alumina Coatings Produced by HVOF and VPS, National Thermal Spray Conference, 20–24 June, Boston, USA, 1994, p. 239.
[22] Y. Liu, T.E. Fischer, A. Dent, Surf. Coat. Technol. 167 (2003) 68.